Pedestal structure and stability of ECRH-only heated plasmas in TCV, comparison with NBI-only heated plasmas

A. Lafay-Labrosse[1], L. Frassinetti[1], B. Labit[2], M. Podestà[2], R. Coosemans[2], A. Stagni[3], A. Perek[2], R. Morgan[2], O. Sundberg[1], S. Saarelma[4], the TCV team*, and The EUROfusion Tokamak Exploitation team**

[1]*Division of Electromagnetics and Plasma Physics, KTH Royal Institute of Technology, Stockholm, Sweden*
[2]*Ecole Polytechnique Fédérale de Lausanne (EPFL), Swiss Plasma Center (SPC), Lausanne, Switzerland*
[3]*Consorzio RFX (CNR, ENEA, INFN, Università di Padova, Acciaierie Venete SpA), Padova, Italy*
[4]*UKAEA Culham, Culham Science Centre, Abingdon, Oxfordshire, OX14 3DB, United Kingdom*
**See the author list of C. Theiler et al 2026 Nucl. Fusion 66 116007*
***See the author list of N. Vianello et al 2026 Nucl. Fusion 66 116010*

1. Introduction

ITER is planned to start research operation with radiofrequency (RF) heating only [1]. The heating scheme can influence plasma parameters that are relevant for the pedestal, such as the normalized plasma beta β_N, the pedestal top density n_e^{ped}, or the normalized separatrix density $n_e^{\mathrm{sep}}/n_e^{\mathrm{ped}}$. Typically, fusion plasmas are heated either by neutral beam injection (NBI) only or by a combination of NBI and RF heating. This work presents a comparison of the pedestal structure and stability between plasmas heated only by NBI and plasmas heated only by electron cyclotron resonance heating (ECRH) in TCV [2]. In DIII-D, it has been shown that the heating scheme (and the localisation of the ECRH deposited power) influences the post-ELM recovery of the pedestal and the pedestal stability via a modification of the peeling-ballooning boundary [3, 4]. In ASDEX-U, small differences have been found in the pedestal structure and transport between ECRH-heated and NBI-heated plasmas [5].

This work relies on experiments performed in TCV at $I_p = 170$kA, $B_t = 1.4$T, high triangularity, without baffle, and without seeding. For the ECRH pulses, the plasma was heated in the core ($\rho_{\mathrm{abs}} \simeq 0.3$) using the third harmonic (X3) in the range 1.3 - 1.6 MW [6]. For the NBI pulses, NBI-1 was used in the range 0.4 - 1.2 MW [7]. Despite the differences in injected power, similar values of absorbed power were obtained with the two heating methods, in the range 0.3 - 1 MW. Different values of gas puffing rate were also used, with a subset characterized by $\Gamma = 0$e/s for both NBI and ECRH pulses.

2. Comparison of two pulses at similar gas rate and absorbed power

In the first place, it is interesting to compare two pulses at similar engineering parameters: #86226 (ECRH-only) and #66294 (NBI-only), with $\Gamma = 0$e/s and $P_{\mathrm{abs}} \simeq 0.5$MW. These pulses have similar $\beta_N \simeq 1.4$ and separatrix electron density $n_e^{\mathrm{ped}} \simeq 10^{19}\mathrm{m}^{-3}$ and same divertor neutral pressure ($p_0^{\mathrm{div}} = 22$mPa).

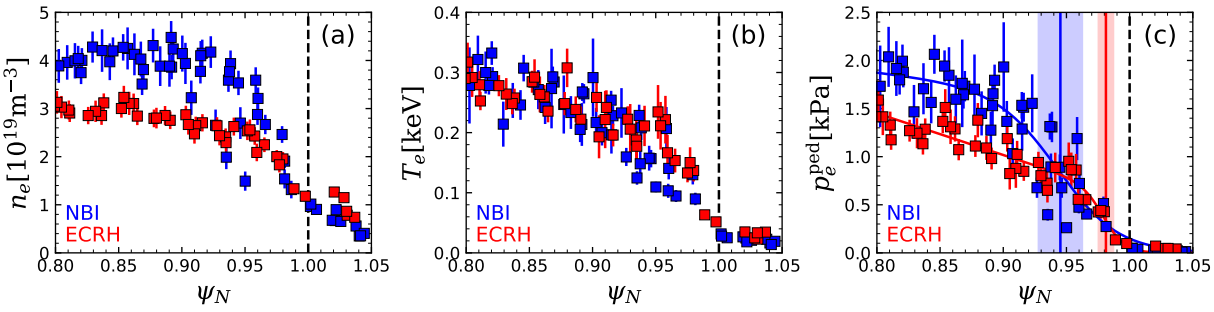

Figure 1. Kinetic pedestal profiles of the NBI-only pulse #66294 (blue) and ECRH-only pulse #86226 (red). *(a)* Electron density, *(b)* Electron temperature, *(c)* Electron pressure. The separatrix is shown with a black line. In frame *(c)*, the position of the maximum gradient is shown with uncertainty.

The kinetic pedestal profiles of the selected pulses are shown in figure 1. It can be seen in figure 1*(a)* that despite both pulses have $\Gamma = 0\mathrm{e/s}$, the density at the pedestal top n_e^{ped} is larger for the NBI pulse. This is likely due to the neutral beams fuelling the core of the plasma ($\Gamma_{\mathrm{NBI}} \simeq 1.5 \times 10^{21}\mathrm{e/s}$), but also possibly due to a difference in pedestal transport between ECRH-heated and NBI-heated plasmas. The pedestal temperature profiles are very similar (figure 1*(b)*). The electron separatrix temperature has been evaluated with the two-point model [8] and, for the both datasets is in the range 56eV – 84eV. Similar pedestal top electron temperature (T_e^{ped}) can be seen. Figure 1*(c)* shows the pedestal pressure profiles of the selected pulses. For NBI, the larger n_e^{ped} and comparable T_e^{ped} implies a larger pedestal top electron pressure p_e^{ped} compared to the ECRH pulses. Interestingly, as shown by the vertical lines in figure 1*(c)*, the position of the maximum pressure gradient is more outward for the ECRH pulse than for the NBI pulse. This can be explained by the fact that both pulses have similar n_e^{sep} but the ECRH pulse has lower n_e^{ped}. Therefore, the position of the maximum density gradient of the ECRH pulse is more outward than in the NBI pulse, and, as consequence, the position of the maximum pressure gradient p_e^{pos} is as well more outward.

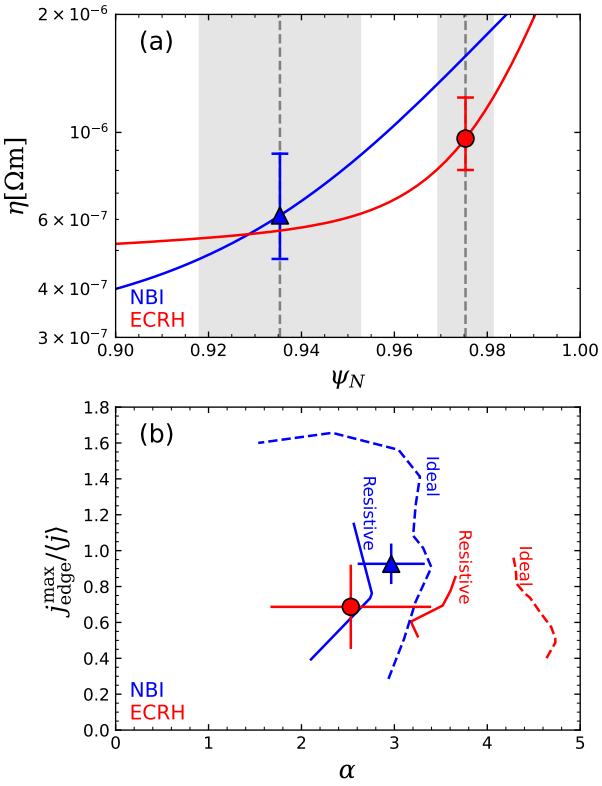

Figure 2. *(a)* Resistivity profiles of the NBI-hated pulse (blue) and the ECRH-heated pulse (red). The circles show the resistivity at the position of the maximum gradient. *(b)* Stability boundaries for the ECRH (red) and the NBI (blue) pulses, for ideal MHD (dashed line) and resistive MHD (full line).

The resistivity profiles and the resistivity at the position of the maximum pressure gradient are shown in figure 2*(a)*. Because $p_e^{\mathrm{pos}}(\mathrm{ECRH}) > p_e^{\mathrm{pos}}(\mathrm{NBI})$, $\eta_{\psi=p_e^{\mathrm{pos}}}$ is larger for ECRH, as shown by the circles in figure 2*(a)*. With this difference in resistivity, it is expected to have stronger resistive effects for the ECRH pulse compared to the NBI pulse. The stability boundaries with ideal and resistive MHD are shown in figure 2*(b)*. The difference in the ideal and resistive boundaries (calculated with MISHKA [9] and CASTOR [10], respectively) is small for the NBI pulse, both being close to the experimental point. For the ECRH pulse, a noticeable difference is seen between ideal and resistive MHD, and the resistive boundary is significantly closer to the experimental point than the ideal one.

3. Effect of the resistivity on the pedestal stability of the high $n_e^{\mathrm{sep}}/n_e^{\mathrm{ped}}$ ECRH-heated pulses

After looking in details at two pulses at similar engineering parameters, the work will now extend the results to the rest of the dataset. Figure 3*(a)* shows the pedestal top quantities for the whole dataset for NBI-only heating and ECRH-only heating. Overall, n_e^{ped} is significantly higher with NBI heating. For NBI, T_e^{ped} is slightly larger and this leads to larger p_e^{ped}. In figure 3*(b)*, it can be seen that $n_e^{\mathrm{sep}}/n_e^{\mathrm{ped}}$ is larger for ECRH compared to NBI, mainly due to the lower n_e^{ped}. Overall, NBI pulses have larger p_e^{ped} and larger normalized pressure gradient α_{exp} compared to ECRH

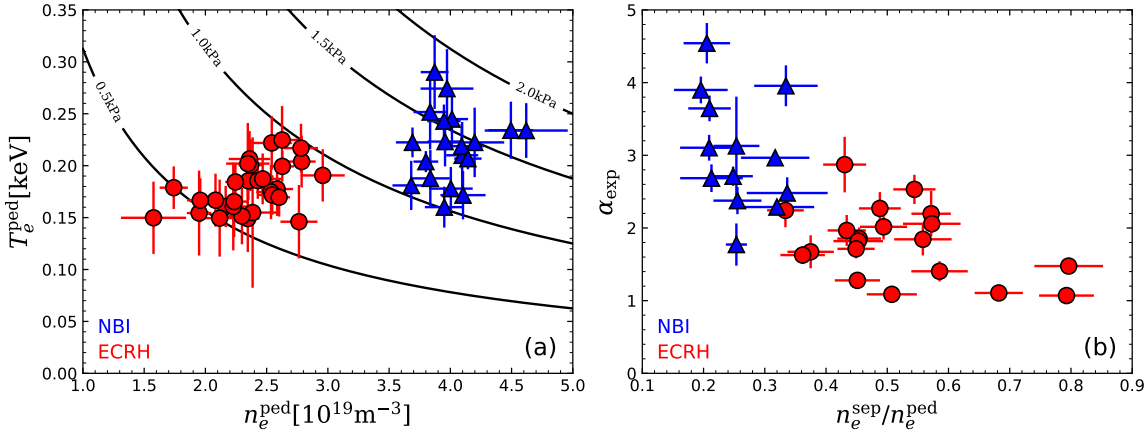

Figure 3. *(a)* T_e^{ped} versus n_e^{ped}. The black lines show the constant p_e^{ped} lines. *(b)* α_{exp} versus $n_e^{\mathrm{sep}}/n_e^{\mathrm{ped}}$. (red: ECRH, blue: NBI).

pulses, and as a consequence the pedestal stability is significantly better for the NBI-heated pulses. It is worth noting that while for some pulse the normalized pressure gradient α_{exp} is comparable between ECRH and NBI pulses, NBI pulses have larger p_e^{ped}. This is due to a wider width with NBI, highlighting a possible difference in pedestal transport between ECRH pulses and NBI pulses.

For this dataset, a reduction of the normalized pressure gradient is seen with increasing $n_e^{\mathrm{sep}}/n_e^{\mathrm{ped}}$ going from NBI pulses to ECRH pulses. This is consistent with previous results from JET [11, 12], where the outward shift of the density pedestal and the following increase in $n_e^{\mathrm{sep}}/n_e^{\mathrm{ped}}$ were correlated with a degradation of the pedestal stability. In JET-ILW, this degradation was linked with the larger pedestal resistivity, and resistive MHD was found to better explain the stability of the high $n_e^{\mathrm{sep}}/n_e^{\mathrm{ped}}$ pulses [12, 13]. The present work introduces a new explanation of the larger resistive effects at higher normalized separatrix density.

In the first place, the increase in $n_e^{\mathrm{sep}}/n_e^{\mathrm{ped}}$ going from NBI to ECRH leads to an outward shift of the position of the maximum gradient p_e^{pos} (see figure 4*(a)*). It is worth reminding that for the ECRH pulses, $n_e^{\mathrm{sep}}/n_e^{\mathrm{ped}}$ is larger due to lower n_e^{ped} (n_e^{sep} being similar). The increase in p_e^{pos} leads to a decrease in the temperature at the pedestal position, and an increase in resistivity at the pedestal position, as shown in figure 4*(b)*. At the position of the maximum gradient, ECRH pulses have larger resistivity than NBI pulses. These results are fully consistent with the results

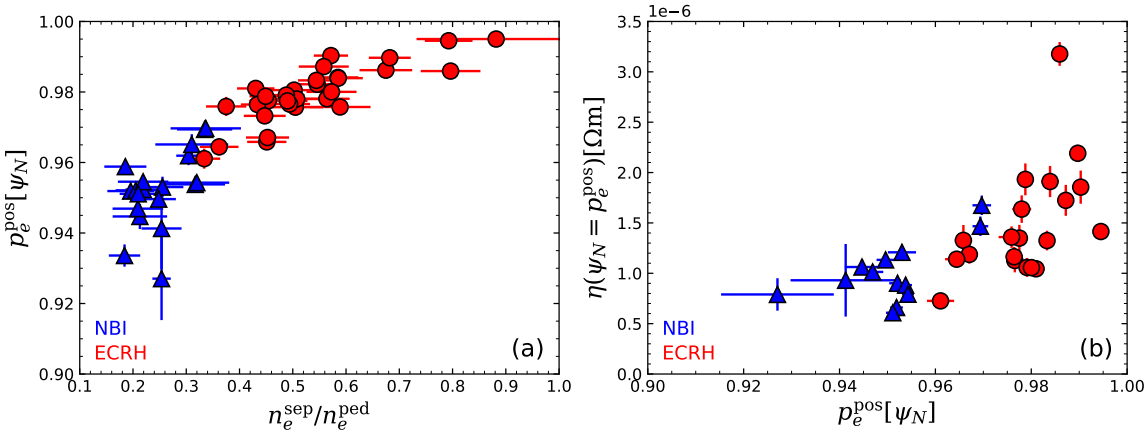

Figure 4. *(a)* p_e^{pos} versus $n_e^{\mathrm{sep}}/n_e^{\mathrm{ped}}$. *(b)* Resistivity at the maximum pressure gradient versus p_e^{pos}. (red: ECRH, blue: NBI).

of section 2, where only two specific pulses were discussed. It has been shown that the ECRH pulses have higher $n_e^{\text{sep}}/n_e^{\text{ped}}$, and that the increase in $n_e^{\text{sep}}/n_e^{\text{ped}}$ is correlated with both an increase in the pedestal resistivity and a worsening of the pedestal stability (with a decrease in α_{exp}). Therefore it is interesting to study the pedestal stability for NBI and ECRH pulses, using both ideal and resistive MHD. The open symbols in figure 5 show the ratio of α_{crit} (marginally stable α at constant parallel current) to α_{exp} for ideal MHD. For the NBI pulses (blue open triangles), the experimental points are close to the stability boundary ($0.5 < \alpha_c/\alpha_e < 1.5$). The ECRH pulses with higher $n_e^{\text{sep}}/n_e^{\text{ped}}$ are far from the ideal MHD stability boundaries ($\alpha_c/\alpha_e \simeq 2.5$). When using resistive MHD instead (full symbols), ECRH and NBI pulses close to the stability boundaries ($0.5 < \alpha_c/\alpha_e < 1.5$). Going from ideal to resistive MHD leads to a clear improvement with experimental data for the ECRH cases, which are limited by resistive MHD instabilities. For the NBI pulses, both ideal and resistive MHD describe well the pedestal stability.

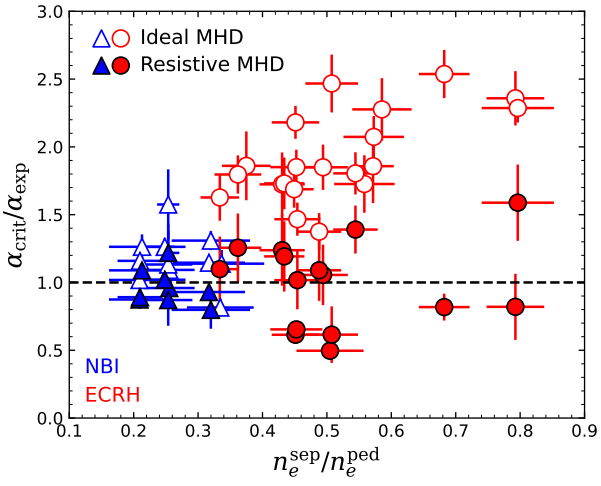

Figure 5. $\alpha_{\text{crit}}/\alpha_{\text{exp}}$ versus $n_e^{\text{sep}}/n_e^{\text{ped}}$ (red: ECRH, blue: NBI – open symbols: ideal MHD, full symbol: resistive MHD).

4. Conclusion

This work presents a comparison of ECRH-only with NBI-only heated plasmas in TCV. The heating scheme influences the pedestal structure, with lower n_e^{ped} and higher $n_e^{\text{sep}}/n_e^{\text{ped}}$ for the ECRH pulses. The larger $n_e^{\text{sep}}/n_e^{\text{ped}}$ is correlated with an outward shift of the pressure maximum gradient and a corresponding increase in resistivity at this position. The ECRH pulses, having higher resistivity, are limited by resistive MHD instabilities in the pedestal, leading to worse pedestal stability. This explains the lower pressure observed in the ECRH dataset. Moreover, this work highlighted possible differences in the pedestal transport between ECRH and NBI pulses. This topic will be investigated in the future by studying the pedestal inter-ELM transport via both experimental observation and gyro-kinetic modelling. Europed pedestal predictions using both ideal and resistive MHD will also shed light on the effect of $n_e^{\text{sep}}/n_e^{\text{ped}}$ on the pedestal stability [14]. Eventually, the Saarelma-Connor model will provide understanding in the difference in pedestal density [15].

This research is supported by Vetenskapsrådet, under Grant Numbers 2023-04895 and by Energimyndigheten under the contract number 2023-204940. This work has been carried out within the framework of the EUROfusion Consortium, partially funded by the European Union via the Euratom Research and Training Programme (Grant Agreement No 101052200—EUROfusion). The Swiss contribution to this work has been funded by the Swiss State Secretariat for Education, Research and Innovation (SERI). Views and opinions expressed are however those of the author(s) only and do not necessarily reflect those of the European Union or the European Commission. Neither the European Union nor the European Commission can be held responsible for them.

References

[1] A. Loarte *et al.* PPCF **67** 065023 (2025)
[2] C. Theiler *et al.* NF **66** 116007 (2026)
[3] S. Banerjee *et al.* NF **61** 056008 (2021)
[4] S. Banerjee *et al.* NF **64** 086010 (2024)
[5] F. Sommer *et al.* NF **52** 114018 (2012)
[6] G. Arnoux *et al.* PPCF **47** 295 (2005)
[7] A. Listopad *et al.* FED **212** 114867 (2025)
[8] Stangeby *The Plasma Boundary of M.F.D.* (2000)
[9] A.B. Mikhailovskii *et al.* PPR **23** 844–57 (1997)
[10] W. Kerner *et al.* JCP **142** 271–303 (1998)
[11] E. Stefanikova *et al.* NF **61** 026008 (2018)
[12] L. Frassinetti *et al.* NF **61** 126054 (2021)
[13] H. Nyström *et al.* NF **62** 126045 (2022)
[14] A. Lafay-Labrosse *et al.* NF **66** 056030 (2026)
[15] S. Saarelma *et al.* NF **64** 076025 (2024)